Int. J. Heat Mass Transfer. Vol. 31, No. 1, pp. 183–195, 1988
Printed in Great Britain

0017–9310/88 $3.00 + 0.00

Developing heat transfer in rectangular channels with rib turbulators

J. C. HAN and J. S. PARK
Department of Mechanical Engineering, Texas A&M University, College Station, TX 77843-3123, U.S.A.

(*Received* 9 *March* 1987 *and in final form* 26 *June* 1987)

Abstract—The combined effects of the rib angle-of-attack and the channel aspect ratio on the distributions of the local heat transfer coefficient for developing flow in short rectangular channels ($L/D = 10$ and 15) with a pair of opposite rib-roughened walls were determined for Reynolds numbers from 10 000 to 60 000. The rib angle-of-attack was varied from 90° to 60°, to 45°, and to 30°, whereas the corresponding channel width-to-height ratio was varied from 1 to 2 and to 4, respectively. Semi-empirical heat transfer and friction correlations were obtained to account for rib angle, rib spacing, channel aspect ratio, rib height and Reynolds number. The results can be used in the design of turbine blade cooling channels.

INTRODUCTION

HEAT TRANSFER enhancement in fully developed turbulent flows in annuli, in circular tubes, and between parallel plates with periodic rib rougheners has been reported [1–6]. The effects of the rib height, the rib pitch, and the rib angle-of-attack on the fully developed average heat transfer coefficient and the fully developed average friction factor over a wide range of Reynolds numbers are well established. Based on the heat transfer and friction similarity laws, semi-empirical correlations have been developed for heat transfer designers.

In some applications, such as gas turbine airfoil cooling design, periodic rib rougheners are cast onto two opposite walls of internal cooling passages to enhance the heat transfer to the cooling air. The sketch of an internally cooled turbine airfoil is shown in Fig. 1(a). The internal-cooling passages can be approximately modeled as rectangular channels with a pair of opposite rib-roughened walls, as shown in Fig. 1(b). Heat transfer and friction characteristics in this kind of rib-roughened channels should be different from those of annuli, parallel-plate channels, or circular tubes. Han *et al.* [7, 8] investigated systematically the effects of the rib configurations on the average heat transfer and friction in the fully developed region in a uniformly heated, straight, square channel with two opposite rib-roughened walls. The results show that the highest heat transfer coefficient, accompanied by the highest friction factor, occurred at rib angles-of-attack between 60° and 75°, whereas the best heat transfer performance for a constant pumping power occurred at rib angles-of-attack between 30° and 45°. These results are primarily obtained for the fully developed turbulent flow in a long square duct with two opposite ribbed walls. The configurations of the internal cooling passages of turbine airfoils are nearly rectangular, however, and are relatively short (typically, $L/D = 10$–15). It is of interest whether the results of the highest heat transfer coefficient (at $\alpha = 60°$ and 75°) and the best heat transfer performance (at $\alpha = 30°$ and 45°) obtained in a long square duct with fully developed flow hold good in the cases of short rectangular channels with two opposite ribbed walls and yet developing flow. Furthermore, from the turbine cooling design point of view, it is very important to know the detailed distributions of the local heat transfer coefficient for developing flow in short rectangular channels with rib turbulators. Therefore, a systematic investigation to determine the effect of the rib angle-of-attack on the local heat transfer distributions in short rectangular channels of different channel aspect ratios should be performed.

The objective of the present study was to investigate the combined effects of the rib angle-of-attack and the channel aspect ratio on the local heat transfer distributions in rectangular channels with two opposite rib-roughened walls for Reynolds numbers from 10 000 to 60 000. The channel length-to-hydraulic diameter ratio (L/D) was varied from 10 to 15. The channel aspect ratio (W/H) was varied from 1 to 2 and to 4. In each channel, the rib turbulators were placed on the top and bottom walls of the test channel (on the channel width, side W) so that the rib turbulators on opposite walls were all parallel with an angle-of-attack of 90°, 60°, 45°, or 30°. The rib height-to-hydraulic diameter ratio (e/D) was varied from 0.047 to 0.078, and the rib pitch-to-height ratio (P/e) was varied from 10 to 20. The local heat transfer distributions on both the smooth side (H) and the rib-roughened side (W) walls from the channel entrance to the downstream region were measured. The local heat transfer data after $X/D > 3$ were averaged and

NOMENCLATURE

a	plenum height
A	heat transfer surface area
b	plenum width
CR	contraction ratio between plenum and test channel, $ab/(WH)$
D	channel hydraulic diameter, $2WH/(W+H)$
e	rib height
e^+	roughness Reynolds number, $(e/D)Re\,(f/2)^{1/2}$
f	friction factor for four-sided ribbed channel
$\bar{f}$	average friction factor in a channel with two opposite ribbed walls
f(FD)	fully developed smooth tube friction factor; also friction factor for four-sided smooth channel
g_c	conversion factor
G	mass flux, $\rho\bar{v}$; also heat transfer roughness function
$\bar{G}$	average heat transfer roughness function
h	heat transfer coefficient
H	flow channel height
K	thermal conductivity of air
l	plenum length
L	test channel length
ΔL	channel length for frictional pressure drop measurement
LHS	left-hand side wall
Nu	Nusselt number, hD/K
Nu(FD)	fully developed smooth tube Nusselt number
Nu_r	ribbed side wall centerline-average Nusselt number for flow in a channel with two opposite ribbed walls
Nu_s	smooth side wall centerline-average Nusselt number for flow in a channel with two opposite ribbed walls
ΔP	pressure drop across the test section
P	rib pitch
Pr	Prandtl number of air
R	friction roughness function
Re	Reynolds number, GD/μ
RHS	right-hand side wall
St	Stanton number, $Nu/(Re\,Pr)$, for flow in a channel with four-sided ribbed walls
St_r	ribbed side wall centerline-average Stanton number for flow in a channel with two opposite ribbed walls
St_s	smooth side wall centerline-average Stanton number for flow in a channel with two opposite ribbed walls
St(FD)	fully developed smooth tube Stanton number
$\overline{St}$	average of the centerline-average Stanton numbers for flow in a channel with two opposite ribbed walls
T_b	bulk mean temperature of air
T_w	local wall temperature
$\bar{V}$	average velocity of air
W	flow channel width
W/H	channel aspect ratio, ribs on side W
X	axial distance from the heated test channel.

Greek symbols

α	rib angle-of-attack
μ	average viscosity of air
ρ	average density of air.

correlated to account for rib angle, rib spacing, and channel aspect ratio. In each channel, the appropriate rib angles-of-attack were identified to establish the highest heat transfer coefficient accompanied by the highest pressure drop, and to obtain the best heat transfer performance for a constant pumping power. First, the experimental program is presented and discussed. Then the semi-empirical correlations are developed, and the heat transfer performance compared.

Additional information on the present investigation is in NASA Contractor Report 4015 by Han *et al.* [9].

EXPERIMENTAL PROGRAM

Experimental apparatus

A schematic of the experimental apparatus is shown in Fig. 2. A 5 hp blower forced air through a settling chamber and a 10.2 cm (4 in.) diameter pipe, equipped with a 3.8 cm (1.5 in.) diameter orifice plate to measure flow rate. A plexiglass plenum was connected between the pipe and the test channel to ensure that the air entering the test channel had a sharp contraction entrance condition (hydrodynamically developing). At the end of the test channel, the air was exhausted into the atmosphere. The Reynolds number based on the channel hydraulic diameter (D) was varied between 10 000 and 60 000.

Both square and rectangular channels were constructed. The square channel had a cross-section of 5.1×5.1 cm (2×2 in.); the rectangular channel I had a cross-section of 10.2×5.1 cm (4×2 in.). The same rectangular channel I also served as the rectangular channel II by changing the channel height (H) from 5.1 cm (2 in.) to 2.55 cm (1 in.). The periodic ribs were placed on the channel width (W) side. The dimensions of the three test channels and the associated plenums

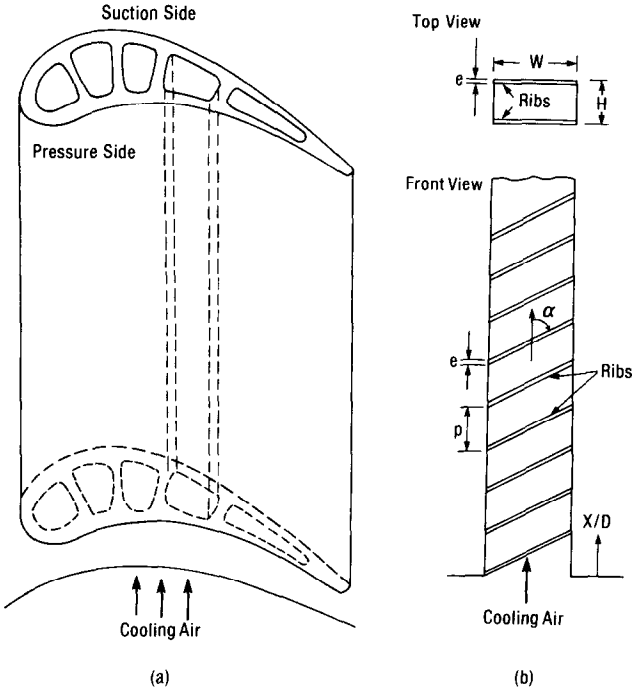

FIG. 1. (a) Sketch of an internally-cooled turbine airfoil. (b) Rectangular channel with a pair of opposite rib-roughened walls.

are shown in Fig. 2. The contraction ratio between the plenum and the test channel was 9 in both the square and rectangular channel I and 18 in the rectangular channel II. These inlet conditions were arbitrarily selected to simulate turbine cooling channels. Note that the actual turbine cooling channels may have a wide range of inlet configurations, which depend on the specific design. Note also that the typical L/D ratios for turbine blades are about 10–15.

The rectangular channel I ($W/H = 2$) consisted of four wood–plexiglass plates, each with a thickness of 1.92 cm (0.75 in.), as shown in Fig. 3(a). Each plate was covered separately by the 0.0025 cm (0.001 in.) thick, stainless steel foil, which was cemented to the inner surface of each plate and controlled individually by a variac transformer, to provide a controllable electrical heating to the test channel. A single strip foil with a width of 4.76 cm (1.875 in.) was used on the channel height (H) side. Three parallel strip foils each with a width of 3.17 cm (1.25 in.), connected in series from one end to the other by the buss bar, were used on the channel width (W) side, as shown in Fig. 3(a). The gap between every two foils was about 0.159 cm (0.0625 in.).

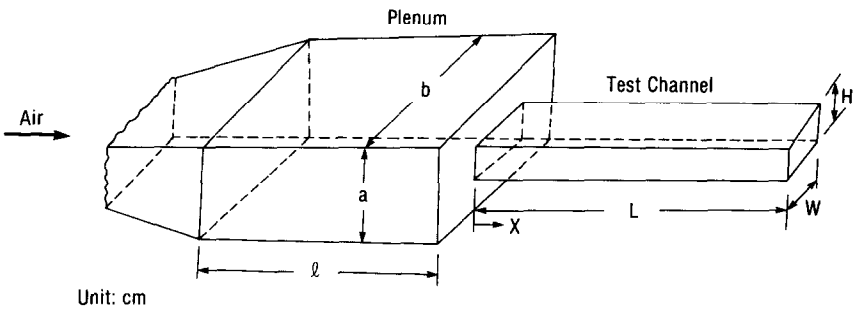

	W	H	W/H	D	L	b	a	CR	ℓ
Square Channel	5.1	5.1	1	5.1	127.5	15.3	15.3	9	15D
Rectangular Channel I	10.2	5.1	2	6.8	127.5	30.6	15.3	9	15D
Rectngular Channel II	10.2	2.55	4	4.08	127.4	30.6	15.3	18	25D

FIG. 2. Dimensions of the test channels and the associated plenums.

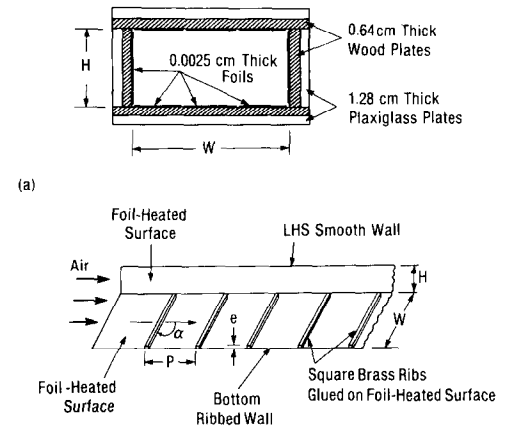

	W/H	e	e/D	P/e	α	Re x 10⁻³
Square Channel	1	0.24	0.047	10 20	90°,60° 45°,30°	10 30 60
Rectangular Channel I	2	0.32	0.047	10 20	90°,60° 45°,30°	10 30 60
Rectangular Channel II	4	0.32	0.078	10 20	90°,60° 45°,30°	10 30 60

(b) Unit : cm

FIG. 3. (a) Cross-section of foil heated test channel. (b) Rib geometries in each test channel.

The rectangular channel II ($W/H = 4$) had the strip foil on the channel height (H) of width 2.22 cm (0.875 in.). The square channel ($W/H = 1$) was constructed in the same way as that of the rectangular channel I, except that a single strip foil with a width of 4.76 cm (1.875 in.) was used separately for each side wall of the channel.

For the cases of ribbed channel tests, the brass ribs of a square cross-section were glued onto the top and bottom plates of the foil-heated channels so that the rib turbulators on opposite walls were all parallel with a required periodic distribution. The rib geometries for each test channel are shown in Fig. 3(b).

The detail of thermocouple locations for each test channel are shown in Fig. 4. The square channel had 180, 36 gauge, copper–constantan thermocouples in strategic locations to measure the local surface temperature. Ninety of these thermocouples were placed on the bottom ribbed wall (channel width side); the other 90 on the right-hand side smooth wall (channel height side). Sixty of each 90 thermocouples were placed along the centerline of the ribbed and the smooth walls. The remaining 30 were well distributed on the middleline and the edgeline of each wall, as shown in Fig. 4. The thermocouple locations were fixed although the rib angle α was varied from 90° to 30°. The thermocouple locations for the rectangular channel I were similar to those of the square channel. To check the symmetry of thermocouple readings on the opposite smooth wall, two thermocouples were placed on the left-hand side smooth wall (LHS), at the downstream region of the rectangular channel I. The same ribbed wall of the rectangular channel I was used for the rectangular channel II. But on the right-hand side smooth wall (RHS) of the rectangular channel II, the thermocouples were placed only along the centerline of the test plate. Note that at the same rib angle α, the rib orientation in the square channel is opposite to that in rectangular channels I and II, as shown in Fig. 4. Each test channel was well insulated with fiberglass. A Fluke 2280 A Data Logger and a TI PC were used for temperature readings and recordings.

Six pressure taps along the centerline of the top ribbed wall and six along the centerline of the LHS smooth wall were used for static pressure drop measurements. Pressure tap locations for each test channel are given in ref. [9]. A pressure tap was also installed in the plenum to check the static pressure of air entering the test channel. A Dywer Microtector with an accuracy up to 0.025 mm (0.001 in.) of water was used for pressure drop measurements in the test channel.

Data reduction

The local heat transfer coefficient was calculated from the local net heat transfer rate per unit surface area from the wall to the cooling air, the local wall temperature, and the local bulk mean air temperature as

$$h = (q - q_{\text{loss}})/[A(T_w - T_b)]. \quad (1)$$

Equation (1) was used for the ribbed side wall and the smooth side wall heat transfer coefficient calculations. The local net heat transfer rate was the electrical power generated from the foil (q), minus the heat loss to the outside of the test channel (q_{loss}). The electrical power generated from the foil was determined from the measured foil resistance and the current through the foil on each plate. The electrical power was also checked with the measured voltage drop across the foil on each plate. In order to place the results on a common basis, the heat transfer area used in equation (1) was always that of a smooth foil on each wall. It was found that the foil provided a nearly uniform heat flux on each wall of the test channel. The maximum heat loss from the ribbed side wall and from the smooth side wall was estimated to be less than 3 and 5%, respectively, for Reynolds numbers greater than 10000. The net heat flux level was varied from about 950 to 2500 W m^{-2} (300–800 Btu h^{-1} ft^{-2}) depending on the test conditions.

The local wall temperature used in equation (1) was read from the output of the thermocouples. The bulk mean air temperatures entering and leaving the test channel were measured by thermocouples. The local bulk mean air temperature used in equation (1) was calculated, assuming a linear air temperature rise along the flow channel. It was checked that the local net heat transfer from the test channel to the cooling air agreed well with the cooling air enthalpy rise along the test channel. The difference between the two

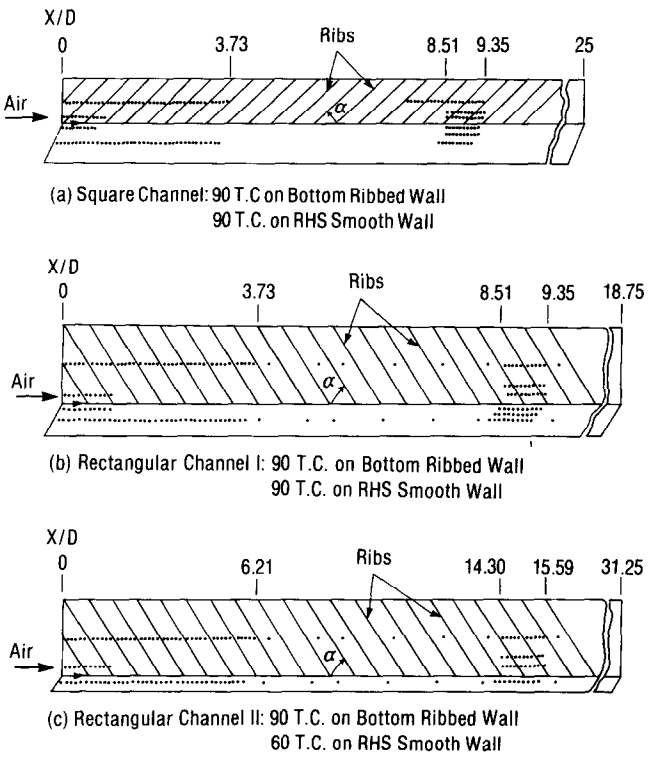

FIG. 4. Detailed thermocouple locations in each test channel.

measurements was estimated to be less than 5% for Reynolds numbers greater than 10 000. The inlet bulk mean air temperature was about 24 to 29°C (75 to 85°F) depending on the test conditions.

The local Nusselt number was normalized using the Nusselt number for fully developed turbulent flow in smooth circular tubes correlated by McAdams as

$$Nu/Nu(\mathrm{FD}) = (hD/K)/[0.023Re^{0.8}\,Pr^{0.4}]. \quad (2)$$

The maximum uncertainty in the Nusselt number was estimated to be less than 8% for Reynolds numbers larger than 10 000 by using the uncertainties estimation method of Kline and McClintock [10].

The pressure drop across the test channel was measured by a microtector. In fully developed channel flow, the average friction factor was calculated from the average pressure drop across the flow channel and the mass flow rate of the air as

$$\bar{f} = \Delta P/\{4(\Delta L/D)\,[G^2/(2\rho g_c)]\}. \quad (3)$$

The average friction factor of the present investigation was based on adiabatic conditions (tests without heating). The maximum uncertainty in the average friction factor was estimated to be less than 9% for Reynolds numbers greater than 10 000.

The average friction factor of the present investigation was normalized by the friction factor for fully developed turbulent flow in smooth circular tubes ($10^4 < Re < 10^6$) proposed by Blasius as

$$\bar{f}/f(\mathrm{FD}) = \bar{f}/[0.046Re^{-0.2}]. \quad (4)$$

EXPERIMENTAL RESULTS

Experimental results for smooth channels

Typical results for the four-sided smooth channels are shown in Fig. 5. In general, the local Nusselt number ratios along the bottom wall (channel width side) and the RHS wall of the test channels exhibit the same trend, except that the local Nusselt number ratios along the RHS wall (channel height side) are slightly higher than those along the bottom wall for rectangular channels I and II. It can be seen that flow separation occurs right after the entrance because of sharp contraction, and then flow reattachment is attained at about $0.5D$ from the entrance, producing a high heat transfer coefficient. At $X/D = 8$–10, for the square channel the Nusselt numbers are about 5–10% higher than McAdams' fully developed turbulent tube flow results ; for the rectangular channels the Nusselt numbers are about 5–15% higher than the fully developed values.

The experimental results from Boelter *et al.* [11] and Sparrow and Cur [12] are included in Fig. 5 for comparison. In ref. [11], the results were obtained for flow in a circular tube with a sharp entrance and heated by condensing steam. In ref. [12], the data were based on the local measurements for flow in a high-aspect-ratio rectangular channel ($W/H = 18$) with a sharp entrance by using the naphthalene sublimation technique. In the developing region with $1 < X/D < 8$, the present data agree qualitatively with those of refs. [11, 12]. In the region with $X/D > 8$, the present data

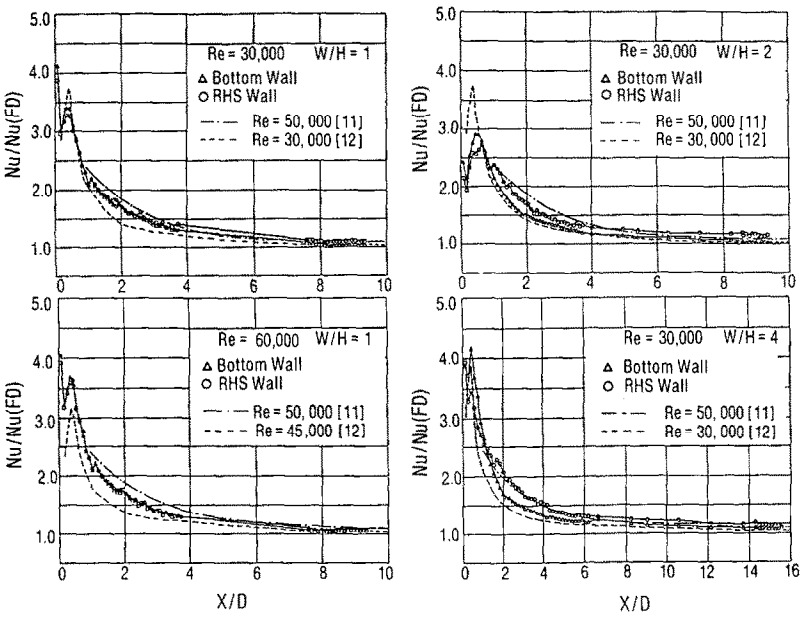

FIG. 5. The local Nusselt number ratio vs X/D in the smooth rectangular channels.

agree fairly well with those of refs. [11, 12]. It is interesting to note that both the present study and ref. [12] show that the flow reattachment is attained at about $0.5D$ from the entrance. These smooth channel results prove that the test sections are reliable to reproduce data for the cases when the periodic ribs are applied.

Experimental results for rib roughened channels

The brass ribs of a square cross-section were glued periodically in-line (parallel) onto the top and bottom walls of the test channels in patterns to achieve the desired spacing and angle-of-attack. In each channel, a total of eight rib geometries (two rib spacings, $P/e = 10$ and 20 ; each rib spacing having four different rib angles-of-attack, $\alpha = 90°$, 60°, 45°, and 30°) were tested respectively for three Reynolds numbers, $Re = 10\,000$, 30 000, and 60 000, as indicated in Fig. 3(b). The detailed raw data for all of the 72 test runs are given in the NASA contractor report 4015 by Han *et al.* [9]. Only the most representative results are presented here.

Local heat transfer coefficient: streamwise distribution

The local heat transfer results are presented as the axial (streamwise) distribution of a normalized Nusselt number ratio, $Nu/Nu(\mathrm{FD})$, as given in equation (2). The local Nusselt number ratios along the centerlines of the ribbed side and the smooth side walls are presented. These centerline Nusselt number ratios are not evenly distributed. In regions where $X/D = 0$–4 and 8–10 for the square and rectangular channel I, and $X/D = 0$–6 and 14–16 for the rectangular channel II, the local Nusselt number was determined at up to five stations for every rib pitch along the axial line for the case of $P/e = 10$ (or ten stations for the case of $P/e = 20$). In regions where $X/D = 4$–8 or 6–14, respectively, the local Nusselt number was determined at only one station for every rib pitch.

Typical results showing the combined effects of the rib angle-of-attack and the channel aspect ratio on the centerline heat transfer coefficients are plotted in Figs. 6–8 for the case of $P/e = 10$ and $Re = 30\,000$ (a total of 12 runs). The test results for $P/e = 20$ and other Reynolds numbers (a total of 60 runs) are given in ref. [9]. In general, the local heat transfer distributions on the ribbed side wall are non-similar with respect to different rib angles-of-attack. In the square channel ($W/H = 1$), the centerline Nusselt number ratio for $\alpha = 90°$ maintains about the same periodic distribution after $X/D > 3$. The periodic distribution of the local Nusselt number ratio is due to flow separation from ribs and flow reattachment between ribs. It can be seen that the periodic Nusselt number ratios for $\alpha = 60°$, 45°, and 30° increase after $X/D > 3$. This implies that, in the square channel, the centerline Nusselt number ratios after $X/D > 3$ for $\alpha = 60°$, 45°, and 30° are higher than those for $\alpha = 90°$, as shown in Fig. 6. The centerline Nusselt number ratios after $X/D > 3$, however, remain at almost the same periodic distribution in the rectangular channel I for all rib angles except $\alpha = 60°$, and in the rectangular channel II for all rib angles, as shown in Figs. 7 and 8.

From the above discussions, one may conclude that the entrance region is quite short ($X/D = 2$–3) in ribbed channels, and the heat transfer coefficient variations track the rib profile. Note that these variations are smoother in real turbine blades because of heat conduction in the rather massive blade wall. However, these variations reflect the actual convection boundary in rib-roughened cooling channels.

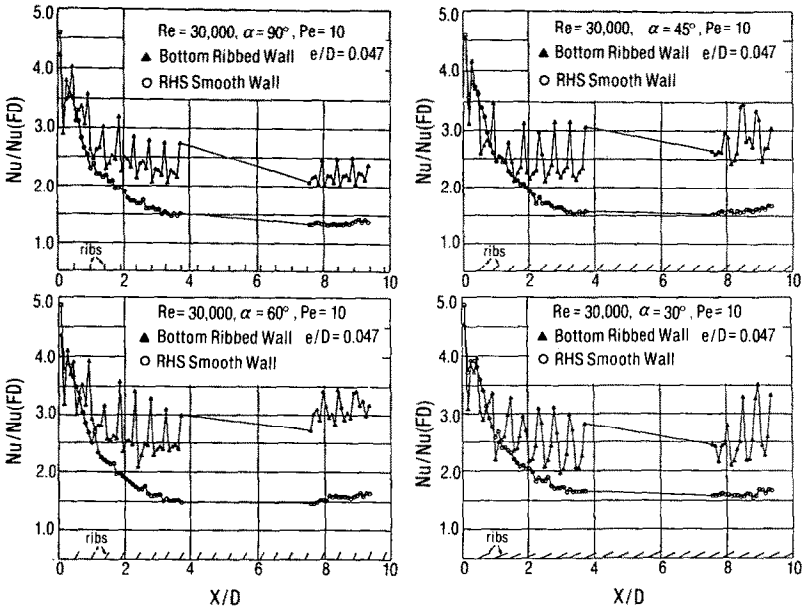

FIG. 6. The effect of rib angle on the centerline heat transfer distribution in the square channel ($W/H = 1$).

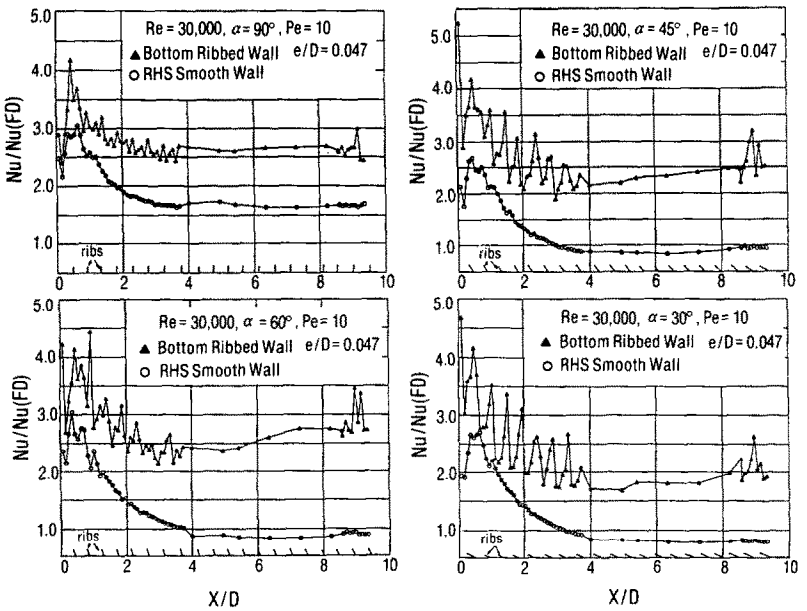

FIG. 7. The effect of rib angle on the centerline heat transfer distribution in rectangular channel I ($W/H = 2$).

Local heat transfer coefficient : spanwise distribution

The suspected secondary flow induced by the angled ribs in each of the test channels is shown in Fig. 9(a). The streamwise-averaged Nusselt number ratio vs the spanwise (lateral) location at $X/D = 8.5$–9.4 and 14.3–15.6 is shown in Fig. 9(b) in each of the test channels for $P/e = 10$ and $Re = 30\,000$. The streamwise-averaged Nusselt number ratio is the average of the periodic Nusselt number ratios along the centerline, the middleline, and the edgeline, respectively, in each of the test channels at the downstream region ($X/D = 8.5$–9.4 in the square channel and rectangular channel I, $X/D = 14.3$–15.6 in rectangular channel II).

In the square channel ($W/H = 1$) for $\alpha = 90°$, the streamwise-averaged Nusselt number ratio on the ribbed side wall is fairly uniform in the lateral position as shown in Fig. 9(b). For $\alpha = 60°$, $45°$, or $30°$ the streamwise-averaged Nusselt number ratio on the ribbed side wall varies in the lateral direction, in that the Nusselt number ratio along the edgeline (right-hand side) is 30–50% higher than that along the centerline. This may be because the secondary flow (or swirling flow) induced by the rib axes moves from the right-hand side to the left-hand side as depicted in Fig. 9(a). Therefore, the Nusselt number ratio on the right-hand side (leading edge side) is higher than that

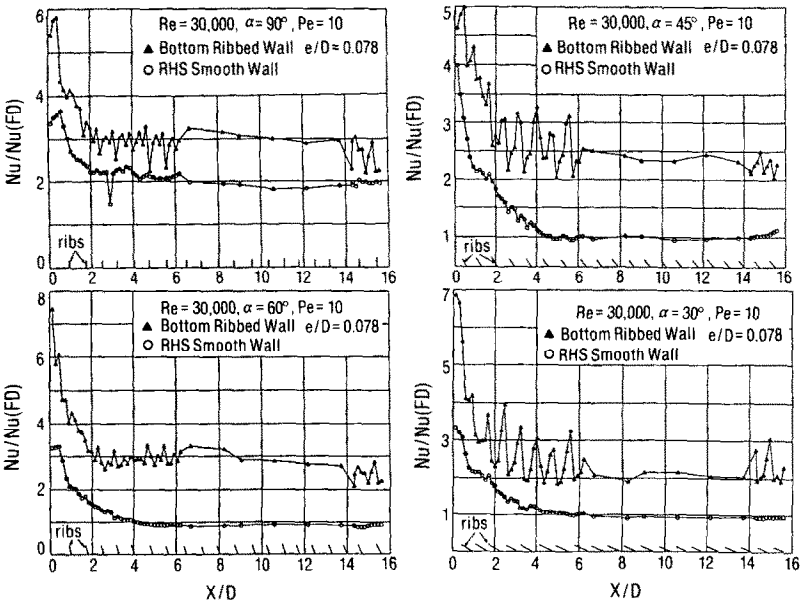

FIG. 8. The effect of rib angle on the centerline heat transfer distribution in rectangular channel II ($W/H = 4$).

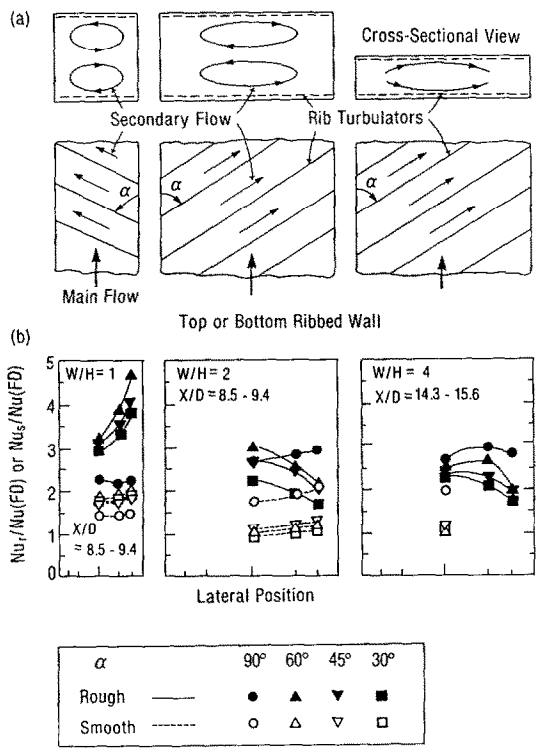

FIG. 9. (a) Effect of rib angle on secondary flow. (b) Effect of rib angle on lateral Nusselt number ratio at $P/e = 10$, $Re = 30000$.

in the centerline and subsequently should be higher than that on the left-hand side (trailing edge side data were not taken). Because of this secondary flow effect, the centerline Nusselt number ratios on both the ribbed side wall and the smooth side wall with angled ribs are higher than that with transverse ribs ($\alpha = 90°$). Similar results are obtained for other Reynolds numbers [9].

In rectangular channel I ($W/H = 2$) shown in Fig. 9(b), for $\alpha = 90°$, the streamwise-averaged Nusselt number ratio behaves similarly to that in the square channel as discussed above. For $\alpha = 60°$, 45°, or 30°, the ribs are oriented so that the secondary flow (or swirling flow) moves along the rib axes from the left-hand side to the right-hand side. Therefore, the Nusselt number ratio on the left-hand side (leading edge side data were not taken) should be higher than that in the centerline and subsequently is higher than that on the right-hand side (trailing edge side). Similar results are obtained for rectangular channel II ($W/H = 4$) as shown in Fig. 9(b). It can be seen that in rectangular channel II, the centerline Nusselt number ratios on both the ribbed side and the smooth side walls for angled ribs are lower than that for $\alpha = 90°$. This may be because the secondary flows induced by angled ribs on both the top and bottom walls of rectangular channel II cancel each other as depicted in Fig. 9(a).

From the above discussions, one may conclude that the rib angle (therefore, the associated secondary flow) has a significant effect on the lateral Nusselt number distribution for the square channel. This effect is gradually reduced for the rectangular channels with higher aspect ratios.

Centerline average heat transfer and friction data

To develop the heat transfer and friction correlations and to compare the heat transfer performance in each channel, the average heat transfer coefficient and friction factor are required. Based on the local heat transfer and the local pressure distribution, it was found that for $\alpha = 90°$, the local Nusselt

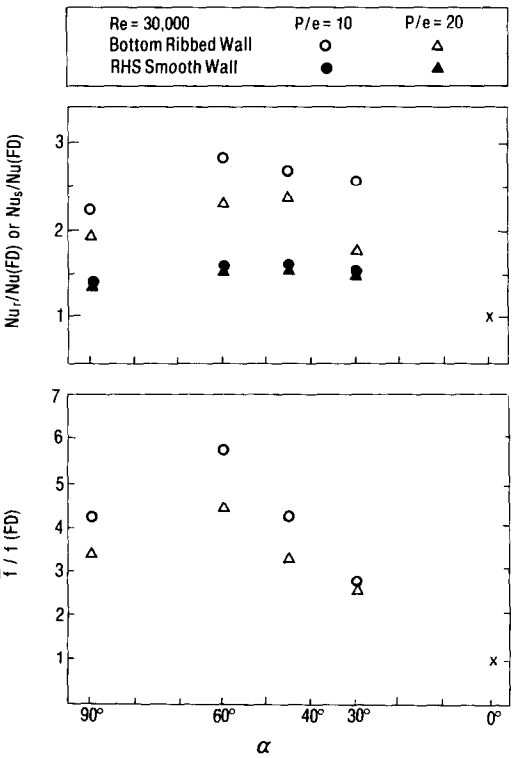

FIG. 10. Heat transfer and friction vs α for square channel.

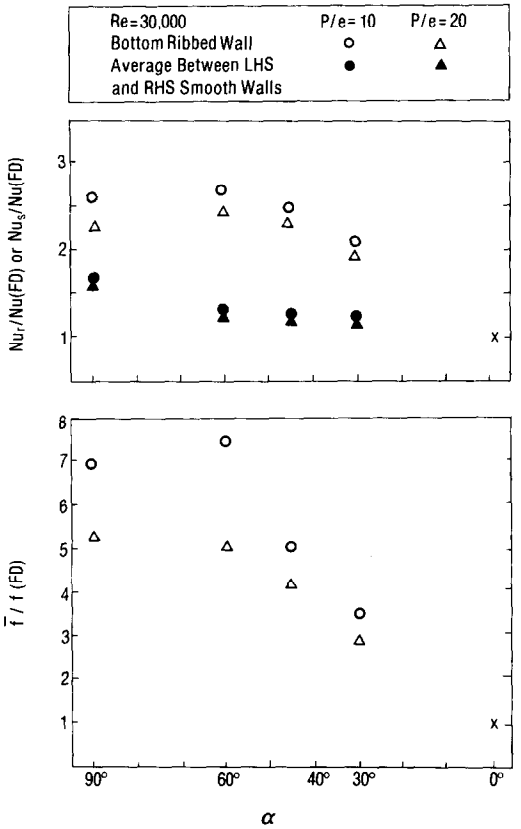

FIG. 11. Heat transfer and friction vs α for rectangular channel I ($W/H = 2$).

number became a periodically developed distribution and the friction factor became a constant value after $X/D > 3$. Therefore, the heat transfer and pressure drop data in the region with $X/D > 3$ in each channel were used to provide the average Nusselt number and the average friction factor. The local pressure distributions in test channels are documented in ref. [9]. The present study, the ribbed-side-wall average Nusselt (or Stanton) number and the smooth-side-wall average Nusselt (or Stanton) number were based on the average value of the centerline Nusselt (or Stanton) number between $X/D = 2.9$–3.7 and 8.5–9.4 for both the square channel and rectangular channel I, and between $X/D = 4.8$–6.2 and 14.2–15.6 for rectangular channel II. These centerline-average Nusselt (or Stanton) numbers were used for heat transfer performance comparison and for correlations discussed in later sections. The ribbed-side-wall centerline-average Nusselt number (Nu_r), the smooth-side-wall centerline-average Nusselt number (Nu_s), and the average friction factor ($\bar{f}$) for all of the 72 test runs are tabulated in ref. [9]. Only the most representative results are discussed here.

Typical results to illustrate the combined effects of the channel aspect ratio and the rib angle on the average heat transfer ratio and on the average friction factor ratio are shown in Figs. 10–12. In the square channel, both the ribbed-side-wall and the smooth-side-wall, centerline-average Nusselt numbers (Nu_r and Nu_s) and the average friction factors ($\bar{f}$) increase with decreasing α and reach a maximum value at $\alpha = 60°$, then decrease with further decreasing α. The results shown in Fig. 10 generally agree with previous data in ref. [8]. In rectangular channel I, both the ribbed-side-wall centerline-average Nusselt number ratios, and the average friction factor ratios increase slightly with decreasing α and reach a peak value at $\alpha = 60°$, then decrease with further decreasing α. In the rectangular channel II, however, both the centerline-average Nusselt numbers and the average friction factors decrease monotonically with decreasing α.

Heat transfer performance comparison

One of the performance evaluation criteria was to compare the increased heat transfer, $[St_r/St\,(\mathrm{FD})]/[\bar{f}/f(\mathrm{FD})]^{1/3}$, or $[\overline{St}/St\,(\mathrm{FD})]/[\bar{f}/f(\mathrm{FD})]^{1/3}$, for the same surface area and pumping power as presented in ref. [8]. The typical results of the effect of rib angle on the increased heat transfer in each channel is shown in Fig. 13 for $e^+ = 200$. The results show that the highest heat transfer for a constant pumping power occurs at $\alpha = 30°$ for the square channel and at $\alpha = 45°$ for rectangular channels I and II. Specifically, in the square channel the increased heat transfer for a constant pumping power at $\alpha = 30°$ is about 30% higher than at $\alpha = 90°$; in rectangular channels I and II, the increased heat transfer at $\alpha = 45°$ is only

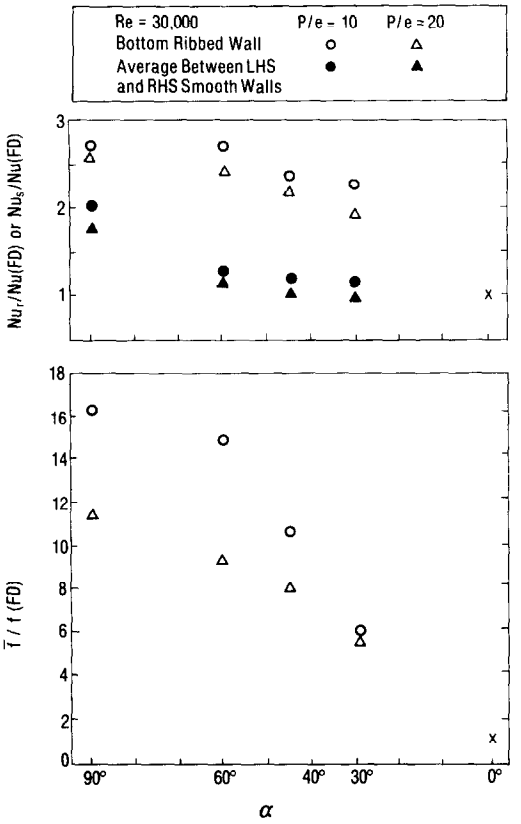

FIG. 12. Heat transfer and friction vs α for rectangular channel II ($W/H = 4$).

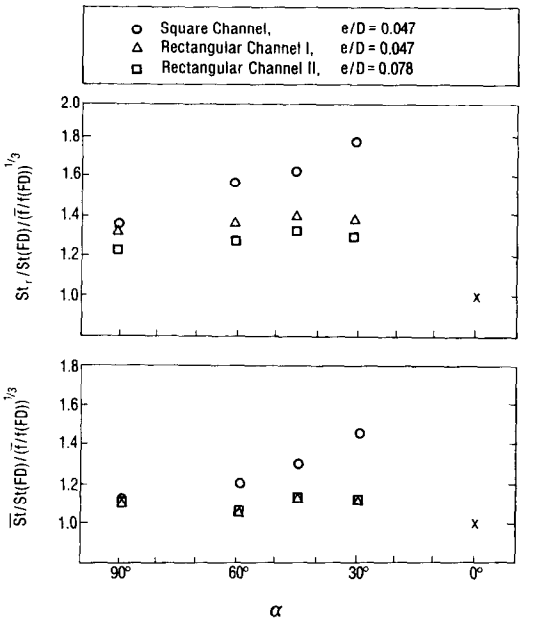

FIG. 13. Increased heat transfer for a constant pumping power vs α in each channel at $e^+ = 200$, $P/e = 10$.

about 5% higher than at $\alpha = 90°$. One can conclude that, in general, the square channel ($W/H = 1$) provides a better heat transfer performance than the rectangular channels ($W/H = 2, 4$). In the square channel, the heat transfer performance increases with decreasing rib angle for a constant pumping power; in the rectangular channels, the dependence of the heat transfer performance on the rib angle is dramatically reduced. Similar results are obtained for other values of e^+ [9].

Heat transfer and friction correlations

For the results of the rectangular channels with turbulence promoters to be most useful for designers, general correlations are required for both the heat transfer and friction over a wide range of parameters, e/D, P/e, α, W/H and Re.

Based on the law of the wall similarity analysis developed in ref. [7] for fully developed turbulent flow in rectangular channels with four-sided ribbed walls, the friction factor, the channel aspect ratio, and the rib height-to-hydraulic diameter ratio should be correlated into a so-called friction roughness function (R) for the geometrically similar roughness as

$$R = (2/f)^{1/2} + 2.5 \ln\{(2e/D)[2W/(H+W)]\} + 2.5. \quad (5)$$

To apply equation (5) for fully developed turbulent flow in rectangular channels with a pair of opposite ribbed walls of the present study (i.e. $X/D > 3$), the friction factor (f) is replaced by the average friction factor ($\bar{f}$, weighted by area), as discussed in ref. [7], by

$$f = \bar{f} + (H/W)(\bar{f} - f(\mathrm{FD})). \quad (6)$$

By substituting equation (6) into equation (5), the friction roughness function of the present study (for $X/D > 3$) can be written as

$$R = \{2/[\bar{f} + (H/W)(\bar{f} - f(\mathrm{FD}))]\}^{1/2} + 2.5 \ln\{(2e/D)[2W/(W+H)]\} + 2.5 \quad (7)$$

where f(FD), the friction factor in smooth rectangular channels, can be approximately calculated from the Blasius equation for smooth circular tubes as

$$f(\mathrm{FD}) = 0.046 Re^{-0.2}. \quad (8)$$

It was found in ref. [7] that the friction factor in smooth circular tubes differed by no more than 4% from smooth square channels and even less from smooth rectangular channels.

Correlation of the present friction data (all of the 72 test runs) is shown in Fig. 14. The data for the non-geometrically similar roughness are displaced because of their different values of α, and P/e. The dependence of R on α, P/e, and W/H for the fully rough region (i.e. $e^+ \geqslant 50$ in the present investigation) shown in Fig. 14 is

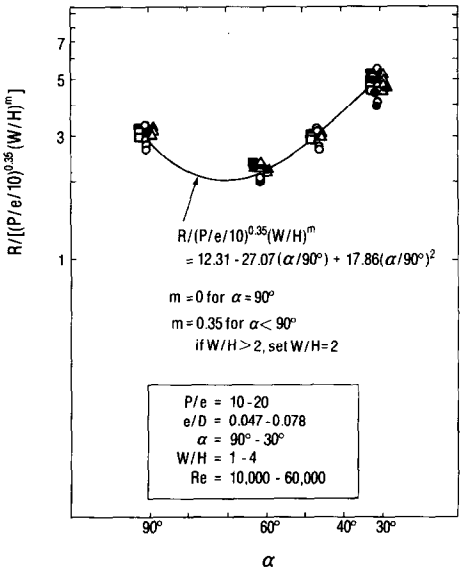

FIG. 14. Final friction factor correlation.

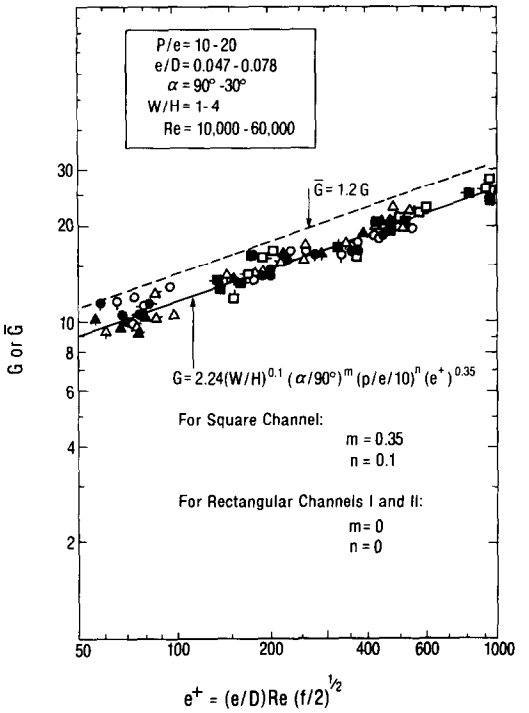

FIG. 15. Final heat transfer correlation.

$$R/[(P/e/10)^{0.35}(W/H)^m] = 12.31 - 27.07(\alpha/90°) + 17.86(\alpha/90°)^2 \quad (9)$$

where

$$m = 0, \quad \text{for } \alpha = 90°$$

$$m = 0.35, \quad \text{for } \alpha < 90°, \quad \text{if } W/H > 2, \quad \text{let } W/H = 2.$$

The deviation of equation (9) is $\pm$ 6% for 95% of the data shown in Fig. 14. Note that R in equation (9) is independent of e^+ (roughness Reynolds number, $e^+ = (e/D)\, Re\sqrt{(f/2)}$). This implies that the average friction factor of the present investigation is almost independent of Reynolds number, i.e. in the fully rough region with $e^+ \geqslant 50$. After R is correlated experimentally from equation (9), the average friction factor ($\bar{f}$) can be predicted by combining equations (7)–(9) for a given e/D, P/e, α, W/H, and Re.

Similarly, in rectangular channels with four-sided ribbed walls, the friction factor, the friction roughness function, and the Stanton number can be correlated into a so-called heat transfer roughness function (G) for the geometrically similar roughness as

$$G = R + [f/(2St) - 1]/(f/2)^{1/2}. \quad (10)$$

To apply equation (10) for rectangular channels with two opposite ribbed walls of the present study (for $X/D > 3$), the friction factor (f) is replaced by equation (6), and the Stanton number (St) replaced by the centerline-average Stanton number on the ribbed side wall (St_r). It is assumed that the ribbed side wall centerline-average Stanton number ($X/D > 3$) may be a constant value either for flow in channels with a pair of opposite ribbed walls, or for flow in channels with four-sided ribbed walls (i.e. assume $St \simeq St_r$ after $X/D > 3$). The heat transfer roughness function G of the present study can then be determined by

$$G = R + \{[\bar{f} + (H/W)(\bar{f} - f(\mathrm{FD}))]/(2St_r) - 1\}/\{[\bar{f} + (H/W)(\bar{f} - f(\mathrm{FD}))]/2\}^{1/2}. \quad (11)$$

Correlation of the present heat transfer data (all of the 72 test runs) is shown in Fig. 15. Very modest dependence of G on P/e and W/H is observed. For a Prandtl number of 0.7 of the present study, the dependence of G on α, P/e, W/H, and e^+ for the fully rough region (i.e. $e^+ \geqslant 50$ in the present investigation) can be represented by

$$G = 2.24\,(W/H)^{0.1}\,(e^+)^{0.35}(\alpha/90°)^m\,(P/e/10)^n \quad (12)$$

for a square channel

$$m = 0.35$$

$$n = 0.1$$

for rectangular channels I and II

$$m = 0$$

$$n = 0.$$

The deviation of equation (12) is $\pm$ 8% for 95% of the data shown in Fig. 15. After G is correlated experimentally from equation (12), the ribbed side wall centerline-average Stanton number (St_r) can be predicted by combining equations (7)–(9), (11), and (12) for a given e/D, P/e, α, W/H, and Re.

The average of the centerline-average Stanton numbers between the smooth side and the ribbed side walls, $\bar{St}$, was calculated from the measured smooth side wall centerline-average Stanton number (St_s) and the ribbed side wall centerline-average Stanton number (St_r). Assuming that equation (11) can be used to

correlate the average of the centerline-average Stanton numbers by replacing G and St_r by $\bar{G}$ and $\overline{St}$, the $\bar{G}$ shown in Fig. 15 can be expressed by

$$\bar{G} = 1.2G. \quad (13)$$

The deviation of $\bar{G}$ is $\pm 10\%$. If G, $\bar{G}$, R, and $\bar{f}$ are known for a given e/D, P/e, α, W/H, and Re, the ribbed side wall centerline-average Stanton number (St_r) and the average of the centerline-average Stanton numbers ($\overline{St}$) can be predicted, respectively, from equation (11) and from the same equation (11) by replacing G and St_r by $\bar{G}$ and $\overline{St}$. After predicting St_r and $\overline{St}$ from correlations, the smooth side wall centerline-average Stanton number (St_s) can be calculated by

$$St_s = \overline{St} + (W/H)(\overline{St} - St_r). \quad (14)$$

CONCLUDING REMARKS

The combined effects of the rib angle-of-attack and the channel aspect ratio on the distributions of the local heat transfer coefficient in short rectangular channels with two opposite rib-roughened walls have been investigated. The following conclusions are drawn.

(1) In the square channel, for $\alpha = 90°$, the periodic Nusselt number decreases in the streamwise direction from the sharp entrance and then reaches a constant periodic distribution after $X/D > 3$; for $\alpha = 60°$, 45°, or 30°, the periodic Nusselt number decreases in the streamwise direction but increases again after $X/D > 3$ because of the secondary flow induced by the rib angle. The periodic Nusselt number remains about the same distribution after $X/D > 3$ in the rectangular channels with $W/H = 2$ (except $\alpha = 60°$) and with $W/H = 4$ for all rib angles.

(2) In each of the test channels, for $\alpha = 60°$, 45°, or 30°, the Nusselt number decreases monotonically along the rib axes (lateral) direction because of the secondary flow induced by the rib angle. The rib angle effect is significant after $X/D > 3$ in the square channel, but the effect is gradually reduced in the rectangular channels with higher aspect ratios.

(3) The highest heat transfer and the accompanying highest pressure drop can be obtained at $\alpha = 60°$ in the square channel; the highest heat transfer and the highest pressure drop occur at $\alpha = 90°$ in the rectangular channel with a channel aspect ratio of 4 ($W/H = 4$). The heat transfer and pressure drop at $\alpha = 60°$ are only slightly higher than at $\alpha = 90°$ in the rectangular channel with a channel aspect ratio of 2 ($W/H = 2$).

(4) The results obtained in the square channel of the present investigation confirm observations in the previous study [8]. The best heat transfer performance in the square channel with angled ribs ($\alpha = 30°$–45°) is about 30% higher than with the transverse ribs ($\alpha = 90°$) for a constant pumping power. The best heat transfer performance in the rectangular channels (with $W/H = 2$ and 4) at $\alpha = 30°$–45° is only about 5% higher than at $\alpha = 90°$ for a constant pumping power basis.

(5) The heat transfer and friction correlations are developed to account for rib spacing, rib angle, channel aspect ratio, rib height, and Reynolds number. The correlations are valid for $e^+ \geqslant 50$, $30° \leqslant \alpha \leqslant 90°$, $0.021 \leqslant e/D \leqslant 0.078$, $10 \leqslant P/e \leqslant 20$, $1 \leqslant W/H \leqslant 4$, and $8000 \leqslant Re \leqslant 80\,000$. The correlations can be used in the design of turbine airfoil cooling passages.

Acknowledgement—This work was funded through Mr Curtis Walker at the U.S. Army–Propulsion Laboratory and was monitored by Mr Robert Boyle at the NASA–Lewis Research Center under contract No. NAS 3-24227. Their support is gratefully acknowledged.

REFERENCES

1. R. L. Webb, E. R. G. Eckert and R. J. Goldstein, Heat transfer and friction in tubes with repeated-rib roughness, *Int. J. Heat Mass Transfer* **14**, 601–617 (1971).
2. J. C. Han, L. R. Glicksman and W. M. Rohsenow, An investigation of heat transfer and friction for rib-roughened surfaces, *Int. J. Heat Mass Transfer* **21**, 1143–1156 (1978).
3. D. L. Gee and R. L. Webb, Forced convection heat transfer in helically rib-roughened tubes, *Int. J. Heat Mass Transfer* **23**, 1127–1136 (1980).
4. R. Sethumadhavan and M. Raja Rao, Turbulent flow heat transfer and fluid friction in helical-wire-coil-inserted tubes, *Int. J. Heat Mass Transfer* **26**, 1833–1844 (1983).
5. L. White and D. Wilkie, The heat transfer and pressure loss characteristics of some multi-start ribbed surfaces. In *Augmentation of Convective Heat and Mass Transfer* (Edited by A. E. Bergles and R. L. Webb). ASME, New York (1970).
6. M. Dalle Donne and L. Meyer, Turbulent convective heat transfer from rough surfaces with two-dimensional rectangular ribs, *Int. J. Heat Mass Transfer* **20**, 582–620 (1977).
7. J. C. Han, Heat transfer and friction in channels with two opposite rib-roughened walls, *ASME J. Heat Transfer* **106**, 774–781 (1984).
8. J. C. Han, J. S. Park and C. K. Lei, Heat transfer enhancement in channels with turbulence promoters, *ASME J. Engng Gas Turbines Pwr* **107**, 628–635 (1985).
9. J. C. Han, J. S. Park and M. Y. Ibrahim, Measurement of heat transfer and pressure drop in rectangular channels with turbulence promoters, NASA Contractor Report 4015 (or AVSCOM Technical Report 86-C-25), 1–197 (1986).
10. S. J. Kline and F. A. McClintock, Describing uncertainties in single-sample experiments, *Mech. Engng* **75**, 3–8 (1953).
11. L. M. K. Boelter, G. Young and H. W. Iversen, An investigation of aircraft heaters—distribution of heat-transfer rate in the entrance section of a circular tube, NACA Technical Note No. 1451 (1948). Data reported by Kays and Crawford in *Convective Heat and Mass Transfer*, 2nd Edn, p. 269. McGraw-Hill, New York (1980).
12. E. M. Sparrow and N. Cur, Turbulent heat transfer in a symmetrically or asymmetrically heated flat rectangular duct with flow separation at inlet, *ASME J. Heat Transfer* **104**, 82–89 (1982).

DEVELOPPEMENT DU TRANSFERT THERMIQUE DANS DES CANAUX RECTANGULAIRES AVEC TURBULATEURS COTELES

Résumé—Les effets combinés de l'angle d'attaque et du rapport de forme du canal sur les distributions du coefficient de transfert thermique local, sont déterminés pour un écoulement évolutif dans des canaux rectangulaires courts (L/D = 10 et 15) avec une paire de parois opposées avec rugosité produite par des cotes, et pour des nombres de Reynolds entre 10 000 et 60 000. L'angle d'attaque des cotes prend les valeurs 90°, 60°, 45° et 30°, tandis que le rapport largeur sur hauteur est égal à 1, 2 et 4. Des formules semi-empiriques de transfert thermique et de perte de charge sont obtenues pour tenir compte de l'angle de la cote, de l'espacement de de la hauteur des cotes, du rapport de forme du canal, du nombre de Reynolds. Les résultats peuvent être utilisés dans la conception des canaux de refroidissement des aubes de turbine.

WÄRMEÜBERTRAGUNG IM EINLAUFGEBIET RECHTECKIGER KANÄLE MIT RIPPENARTIGEN VERWIRBELUNGSEINBAUTEN

Zusammenfassung—Die kombinierten Einflüsse von Rippenanstellwinkel und Seitenverhältnis des Kanals auf die Verteilung des örtlichen Wärmeübergangs-Koeffizienten im Einlauf kurzer rechteckiger Kanäle (L/D = 10 und 15) mit einem Paar gegenüberliegender berippter Wände wurden für Reynolds-Zahlen von 10 000 bis 60 000 untersucht. Der Rippenanstellwinkel wurde von 90° über 60°, 45° bis 30° variiert, das Verhältnis von Breite zu Höhe des Kanals von 1 über 2 bis 4. Halbempirische Korrelationen für Wärmeübergang und Widerstand wurden in Abhängigkeit von Rippenanstellwinkel, Rippenabstand, Seitenverhältnis, Rippenhöhe und Reynolds-Zahl ermittelt. Die Ergebnisse können bei der Konstruktion von Kühlkanälen in Turbinenschaufeln benutzt werden.

НЕУСТАНОВИВШИЙСЯ ТЕПЛОПЕРЕНОС В ПРЯМОУГОЛЬНЫХ КАНАЛАХ С РЕБРИСТОЙ ТУРБУЛИЗИРУЮЩЕЙ ПОТОК ШЕРОХОВАТОСТЬЮ

Аннотация—В диапазоне значений числа Рейнольдса 10 000–60 000 исследовано совместное влияние угла атаки ребра и отношения сторон на распределения локального коэффициента теплообмена при неустановившемся течении в коротких прямоугольных каналах (L/D = 10 и 15), две противоположные стенки которых имели шероховатость в виде ребер. Углы атаки ребер изменялись от 90° до 60°, 45° и 30°, а отношение ширины к высоте канала изменялось соответственно от 1 до 2 и 4. Получены полуэмпирические зависимости для теплообмена и трения, учитывающие угол наклона и высоту ребра, расстояние между ребрами, отношение сторон канала и число Рейнольдса. Результаты могут использоваться для расчетов охлаждающих каналов лопаток турбин.